Geotech Geol Eng
https://doi.org/10.1007/s10706-024-02850-0

ORIGINAL PAPER

Experimental Study on Acoustic Emission Properties and Damage Characteristics of Basalt Exposed to High Temperature Treatment

Wenzhao Chen · Rong Hu · Xiqi Liu · Gang Wang · Bingwen Gong · Yan Chang · Heng Deng · Chunming Qi

Received: 3 February 2024 / Accepted: 7 June 2024

Abstract To study the damage and acoustic emission (AE) energy evolution of basalt under high temperature, a series of tests under uniaxial stress are carried out on basalt heated at 25 °C, 200 °C, 400 °C, 600 °C, 800 °C and 1000 °C. Through the comprehensive analysis of AE parameters such as absolute energy and amplitude, the AE characteristics and damage evolution laws of basalt were explored. The results show that high temperature has a significant effect on the characteristics of rock stress–strain curve. With the increase of temperature, the compaction stage of the curve becomes longer, the plasticity increases, and the peak strength of basalt decreases. The higher the heat treatment temperature, the faster the strength decreases, and the strength decreases by 63.91% at 1000 °C. The AE localization points converge from the dispersed state to the aggregated state. With the increase of temperature, the period of convergent nucleation of the AE localization sites is advanced, high amplitude AE signals shifted from a concentrated distribution near the peak stress to a discrete distribution throughout the entire process. The heat treatment of the rock has an additive effect on the burstiness. 600–800 °C can be used as the threshold temperature of basalt to transform from brittle failure to plastic failure. The high temperature effect is responsible for the transition of the AE cumulative absolute energy at 400–600 °C. The influence of high temperature on damage evolution is discussed. The initial damage increases exponentially after 800 °C. With the increase of temperature, the evolution rate of damage variable becomes faster and gradually changes from linear to nonlinear.

Keywords High temperature · Uniaxial compression · Basalt · Damage evolution · AE energy evolution

W. Chen · R. Hu · C. Qi
School of Civil Engineering, University of South China, Hengyang 421001, Hunan, China

R. Hu · X. Liu (✉) · Y. Chang · H. Deng
Pearl River Water Resources Research Institute, Guangzhou 510611, Guangdong, China
e-mail: Liu-Xiqi@whu.edu.cn

G. Wang
School of Civil Engineering, Shaoxing University, Shaoxing 312000, Zhejiang, China

B. Gong
China Seventh Bureau of Water Conservancy and Hydro Power Engineering, Chengdu 610000, Sichuan, China

1 Introduction

With the continuous improvement of the modern energy system, the disaster-causing mechanism of engineering activities and disaster warning and risk assessment have become the core scientific issues. Underground engineering activities such as deep mineral exploitation, geothermal resource development, underground coal gasification and nuclear waste

Published online: 22 June 2024

repository are all involved in the damage of high-temperature rocks (Horst 2019; Zhao 1994; Ozguven and Ozcelik 2013; Luc et al. 2015; Jobmann et al. 2010; Ju 2010). We have to consider the effect of high temperature on the mechanical properties and deformation behavior of rock materials. Therefore, the study of rock failure characteristics and damage evolution law after high temperature plays a very important role in the selection of engineering structural parameters, scientific evaluation of engineering rock mass stability and nuclear waste storage safety.

Rock thermal effect has been widely studied as a research hotspot, but it mainly focuses on the physical properties and mechanical behavior of different types of rocks, such as elastic modulus (Justo and Castro 2020; Motra and Stutz 2018), compressive strength (Justo and Castro 2020; Hakan et al. 2019; Deng et al. 2022), longitudinal wave velocity (Vagnon et al. 2021; Deng et al. 2022), density (Hrifech et al. 2023; Motra and Stutz 2018) and Justo and Castro (2020) studied the influence of temperature on the fracture characteristics of sandstone, limestone and marble, and obtained the relationship between physical and mechanical parameters and temperature change. Vagnon et al. (2021), Hrifech et al. (2023), Motra and Stutz (2018) and other scholars have conducted in-depth research on the physical and mechanical behavior of rock under the influence of high temperature, and revealed the relationship between physical properties and heat-induced damage. Deng et al. (2022) studied the effect of high temperature on the physical and mechanical properties of granite, and analyzed its dynamic damage evolution law. It can be seen that with the increase of temperature, the physical and mechanical properties decreased, the damage increased, and the AE activity was severe. AE technology can monitor the deformation instability process of thermally treated rocks under external stress in real time (Rong et al. 2018), so it is widely used in experiments. Li et al. (2021) studied the deformation and failure characteristics of marble and the AE activity rule at 30 °C, 60 °C, 90 °C, 120°Cand 150 °C, revealing the relationship between the failure characteristics of marble and temperature. Yin et al. (2022) conducted heat treatment on granite samples at 25 °C, 200 °C, 400 °C, 600 °C and 800 °C. Based on brittleness index and peak strain energy, the relationship between temperature and energy evolution of granite was discussed, revealing that high temperature leaded to energy dissipation and reduced rock brittleness. Kumari et al. (2017) investigated the stress–strain behaviour under temperature conditions by conducting a series of high-temperature tri-axial experiments on Australian Strathbogie granite under four different temperatures (RT, 100, 200, 300 °C), and monitored the process by AE. The mechanical behaviour in the process of rock failure was analyzed.

The above research results have systematically studied the physical and mechanical properties of different rocks and obtained many useful conclusions. At the same time, the generation of cracks under high temperature will destroy the integrity of rock and affect the rock composition and mineral cementation form, which is very likely to destroy the stability of underground rock mass engineering (Ali and Bradshaw 2010; Manish et al. 2017; Víctor et al. 2021). Therefore, it is particularly necessary to study the damage characteristics and failure mechanism of rock after high temperature. In addition, basalt is often selected as the basic material for nuclear waste storage (Thomas 1983). During the disposal process, nuclear waste continuously releases heat in the form of nuclear decay heat. High temperature will not only cause thermal stress in the rock due to thermal expansion, but also change the physical and mechanical properties of the rock, as well as the deformation and failure mechanism (Kwon and Choi 2006; Ren et al. 2019; Nakayama et al. 2011; Kitamura et al. 2011). Therefore, the revelation of the mechanical properties and damage evolution of basalt at high temperature has certain guiding significance for the key technical problems of rock mass engineering under high temperature such as nuclear waste storage safety.

Based on the above analysis, to fully investigate the effects of high temperature on the fracture process and the failure mechanisms of rocks under compressive stress, this study conducts a series of uniaxial compression tests on thermally treated basalt using the AE monitoring technology. Firstly, the effect of high temperature on the mechanical properties of basalt was studied. Secondly, the relationship between AE parameters such as absolute energy and amplitude and temperature is comprehensively analyzed, and the temporal and spatial evolution of AE events and damage variables are used to study the damage evolution law. In summary, the failure mechanism of

thermally damaged basalt is revealed by analyzing the AE mechanical characteristics, damage evolution law and failure pattern of the samples.

2 Experimental Procedure

2.1 Sample Preparation and Test System

Standard cylindrical basalt samples with a diameter of 50 mm and a height of 100 mm specified by the International Society of Rock Mechanics (ISRM) (Fairhurst and Hudson 1999) are used in the test, as shown in Fig. 1. The basic physical and mechanical parameters of basalt without temperature treatment are shown in Table 1.

The MTS 815 high-rigidity rock mechanics test system is used in this loading test. The system consists of a test part, a loading part and a control part. It is equipped with a servo-controlled full-automatic pressurization and measurement system. The vertical maximum output is 4600kN. The overall stiffness of the test frame is 11.0×10^9 N/m. The structure of the test machine is shown in Fig. 2. The DIC test system of MatchID company and the PCI-II AE test system of American Physics Acoustic Company (PAC) are synchronously applied. The threshold value is set to 40 dB, the pre-gain is 40 dB, the sampling frequency is 1 MHz, and the AE sensor type is RT50-AE, as shown in Fig. 3.

2.2 Test Design

Based on Standard for Test Methods of Engineering Rock Mass (GB/T 50266-2013), the basalt samples are dried at 105 °C for 24 h. The selected samples are treated at high temperature (200 °C, 400 °C, 600 °C, 800 °C, 1000 °C) by KSL-1200 X muffle furnace, and heated to the specified temperature at a rate of 10 °C/min.

After maintaining the corresponding temperature for 2 h, the power supply is cut off, and the samples are placed in the furnace and cooled to room temperature. Subsequently, the uniaxial compression test is carried out on the MTS 815 high-rigidity rock mechanics test system to obtain the stress–strain curve. At the same time, AE sensors are installed on rock samples to monitor the AE signals in the process of basalt compression deformation in real time.

Table 1 Basic physical and mechanical parameters of basalt

Density/g m^{-3}	v_p/m s^{-1}	E/MPa	σ/MPa	Poisson's ratio
2.90	5987.54	271.98	194.95	0.1

v_p is longitudinal wave velocity; E is elasticity modulus; σ is uniaxial compressive strength

3 Result

3.1 Stress–Strain Relationship

The stress–strain curves of basalt after different temperature treatments are shown in Fig. 4.

Similar to that at room temperature, the complete stress–strain curve of high temperature basalt under uniaxial compression after cooling roughly goes through four stages: compaction, elasticity, yield and

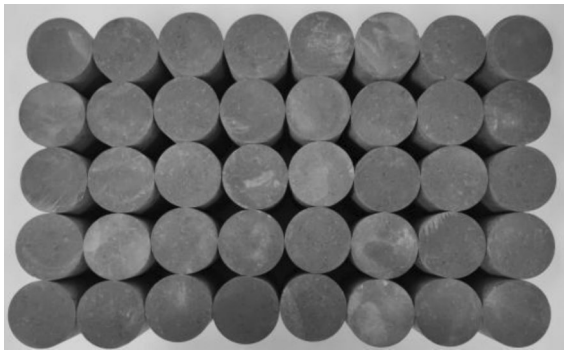

Fig. 1 Basalt sample

Fig. 2 MTS 815 high rigidity rock mechanics test system

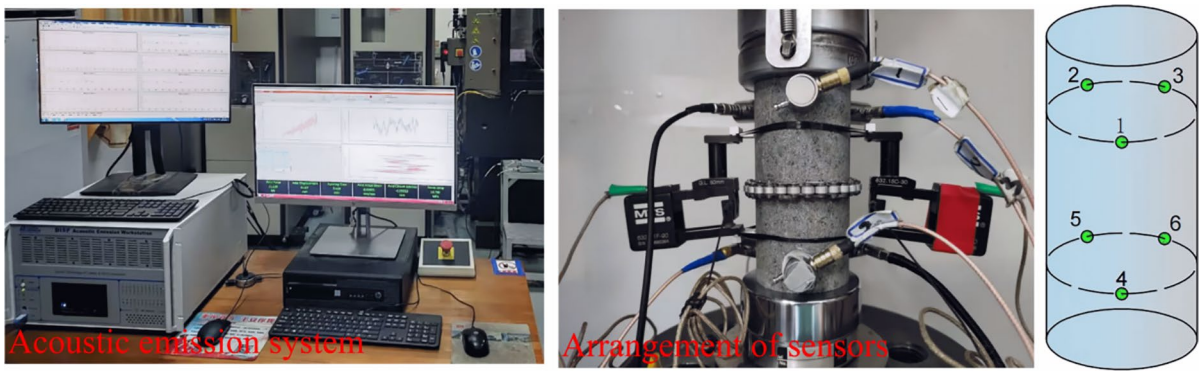

Fig. 3 AE signal analyzer

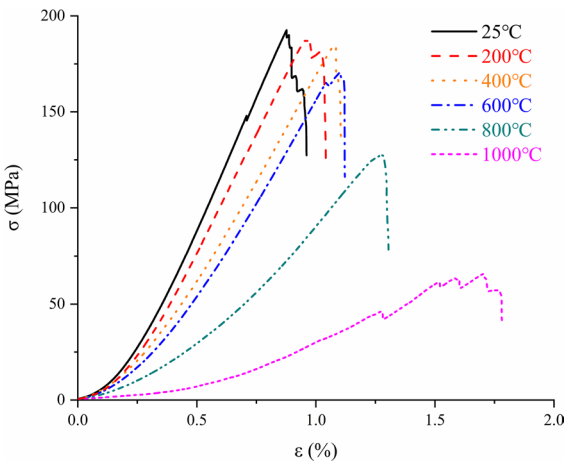

Fig. 4 Stress–strain curve of basalt after different temperature treatment

failure, as shown in Fig. 4. In the compaction stage, the curve is concave. The higher the temperature, the longer the compaction stage, indicating that the higher the temperature, the more initial micro-cracks inside the rock. With the increase of temperature, the slopes of linear elastic stage are 278.83, 244.89, 201.81, 196.72, 108.76 and 48.85, respectively, showing a decreasing trend. When the temperature reaches 1000 °C, the plastic yield stage is obvious, and a yield platform appears. Finally, the rock enters the failure stage, at which the axial stress reaches the peak strength. Before 800 °C, the rock sample is destroyed rapidly, the axial stress decreases sharply, and the strain changes very little, showing brittle failure. However, at 1000 °C, the rock sample has stress fluctuation during the failure process, showing obvious plastic characteristics. This is because the high temperature of 1000 °C causes a large number of thermal cracks in the rock, resulting in multiple penetrations of thermal cracks during the loading process, showing multiple stress decreases. With the increase of temperature, the peak strength is 192.56 MPa, 188.70 MPa, 185.04 MPa, 170.54 MPa, 127.63 MPa and 65.64 MPa, respectively, showing a decreasing trend. Due to the difference in thermal expansion of different particles of minerals inside the rock, structural thermal stress will be formed between the particles, thereby forming more new cracks or promoting the expansion of primary cracks, resulting in the deterioration of the mechanical properties of basalt and the reduction of strength.

3.2 Analysis of AE Characteristics

3.2.1 AE Energy and Three-Dimensional Spatio-temporal Evolution Laws

The stress–strain behavior of rock has a good correspondence with the damage types and AE energy evolution of rock (Sagar and Prasad 2012; Xue et al. 2021; Khadivi et al. 2023). The damage represented by AE energy has good reliability, which can reflect the essential characteristics of rock damage and fracture (Wang et al. 2023; Ullah et al. 2023). The spatial–temporal evolution of the AE events can directly visualize the development of cracks inside the rock samples during the process of rockburst incubation (Chajed and Singh 2024; Singalreddy et al. 2022). Figure 5 shows the evolution of AE energy and three-dimensional spatio-temporal localization during the

whole process of uniaxial compression of basalt after high-temperature action. Three-dimensional display is carried out according to the amplitude and occurrence time of AE source. Among them, the amplitude of AE source (unit: dB) is distinguished by the size and color of the ball. The larger the amplitude of AE, the larger the size and the deeper the color of the ball.

As shown in Fig. 5, the damage process of rock samples is divided into three stages: the initial damage stage (0–20% σ_c), the stable damage development stage (20% σ_c–60% σ_c), and the accelerated damage development stage (60% σ_c–σ_c) based on the AE three-dimensional spatio-temporal evolution (Li et al. 2022; Cao et al. 2022). In the initial damage stage, the primary cracks and pores within the rock are closed, the AE energy is increased slightly, and the AE sources are randomly distributed in the specimen. During the stage of stable damage development, the pressure on the rock samples is insufficient to cause the formation of new cracks, resulting in little AE energy activeness. Essentially, the cumulative AE energy curves are horizontal. At the peak stress of about 60% σ_c, the number of AE localization points increases slightly, indicating crack initiation. In the early stage of accelerated damage development, the AE localization points are gradually aggregated and connected at about 80% σ_c, and initially converge to form a nucleus, which indicates that cracks begin to expand and small damages gradually accumulate. In the late stage of accelerated damage development, the number of AE localization points increases dramatically, and a large number of localization points in the initial nucleation areas are converged into rupture zones, indicating continuous crack expansion and penetration accompanied by the generation of a large number of new cracks, and the AE source is extremely active. The cumulative AE energy curves show a sudden increase change approximate to a vertical line.

Compared with the room temperature, with the increase of heat treatment temperature, the nucleation period of acoustic emission localization point is advanced. The AE energy fluctuates before the stress peak, and no longer maintains a small energy state, suggesting that the heat treatment of the rock has an additive effect on the burstiness, which is most pronounced when the temperature is 1000 °C. The turning point of the cumulative AE absolute energy curve is delayed, and there is a corresponding "step-like" change. In addition, the peak absolute energy of the AE shows a hysteresis phenomenon compared to the peak stress.

Differences in heat treatment temperatures lead to differentiation in the initial thermal damage of the specimen, which alters the course of damage evolution during specimen destruction, resulting in different rock damage patterns. When the heat treatment temperature increases from 25 to 1000 °C, the time required for the basalt sample cracks from complete development to failure is 2396 s, 2930 s, 3239 s, 3315 s, 3830 s and 5127 s, respectively, showing an increasing trend, and the rock failure shows a transition from brittle failure to plastic failure. The number of AE event points is 718, 1314, 2278, 4048, 8375 and 9193, respectively, showing an increasing trend. 600–800 °C can be used as the threshold temperature of basalt to transform from brittle failure to ductile failure. The transformation of basalt failure pattern changes the damage evolution and development course of sample in the failure process, and affects the course of crack initiation, condensation, nucleation and penetration failure, leading to the difference of three-dimensional spatio-temporal evolution.

The high temperature affects the rock energy release process to a certain extent, and there are some differences in the AE absolute energy and cumulative absolute energy evolution laws for rock samples under different high temperature. The peak and cumulative absolute energy of AE after different thermal temperature are shown in Table 2.

As can be seen from Figs. 6 and 7, with the increase of heat treatment temperature, the peak of AE absolute energy shows a trend of first decreasing, then increasing, and then decreasing. The cumulative absolute energy of AE shows a trend of first increasing and then decreasing. The obvious turning point of absolute energy and cumulative absolute energy of AE occurs at 400–600 °C, so this temperature range can be considered as the turning point of absolute energy of AE. However, at 1000 °C, an order of magnitude decrease in the AE absolute energy and cumulative absolute energy occurs due to the change of failure pattern. This phenomenon is mainly due to the fact that heat treatment at a certain temperature (200–400 °C) is helpful to improve the properties of basalt. At a relatively low temperature, heat treatment mainly causes dehydration of the sample and expansion of the mineral grain. However, the degree

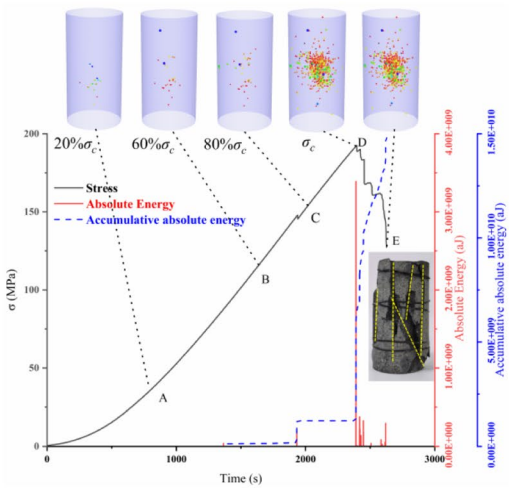

(a) 25℃

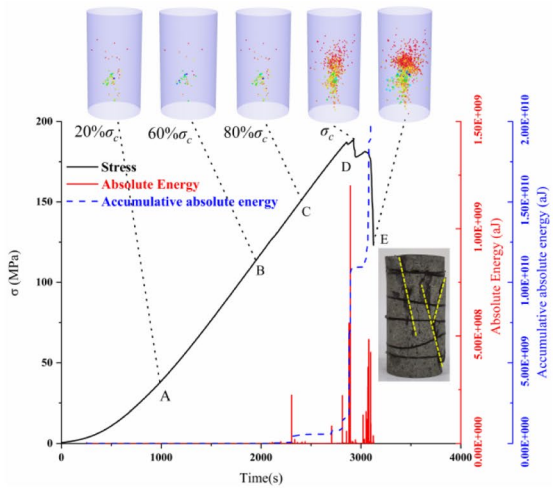

(b) 200℃

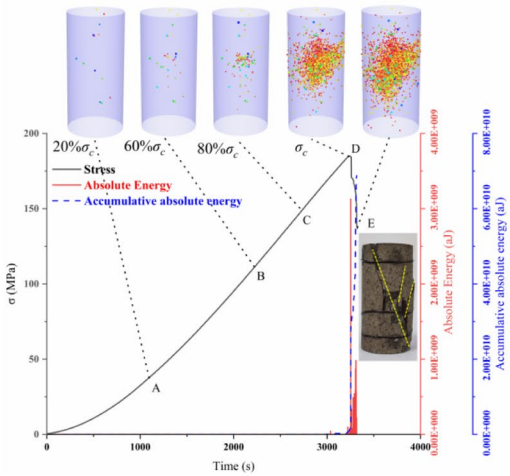

(c) 400℃

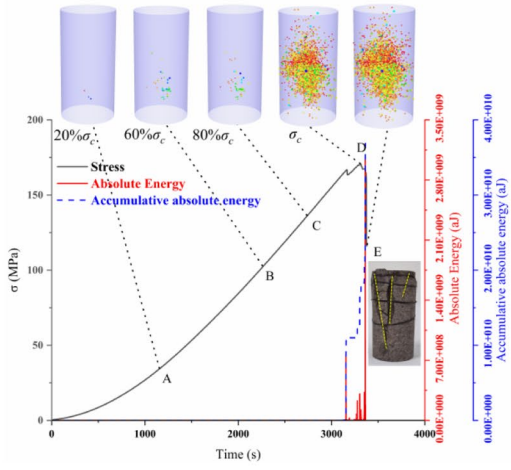

(d) 600℃

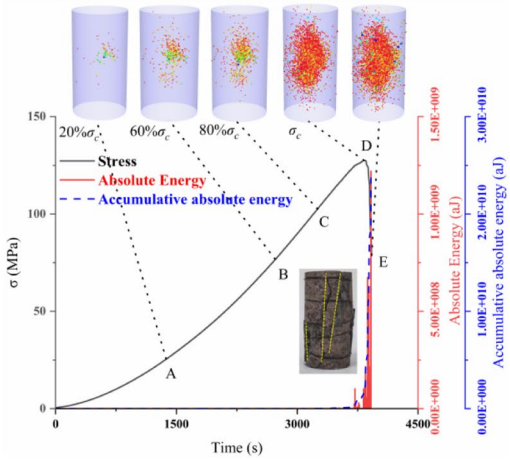

(e) 800℃

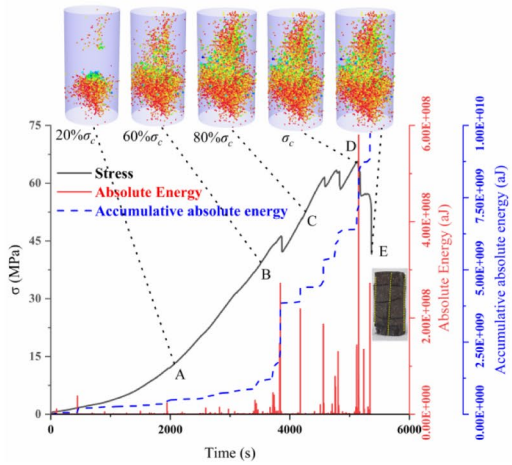

(f) 1000℃

◂**Fig. 5** AE energy and three-dimensional spatial–temporal evolution of basalt

of thermal expansion will not cause the thermal fracture of mineral grains and the further expansion of existing natural cracks. Instead, some natural cracks are gradually closed, and the contact between mineral grains is closer, releasing more elastic strain energy (Ma and Chen 2020; Xie et al. 2023; Dong et al. 2022). However, at 400–600 °C, the mineral particles of basalt begin to deform, and even the minerals begin to decompose, transform and recrystallize under high temperature, which consumes more elastic strain energy. Secondly, with the increase of temperature, the AE activity becomes more and more intense, and the elastic strain energy consumed by the slip and rotation of mineral particles under compressive load is also increasing.

3.2.2 Amplitude Distribution Characteristics of AE

AE amplitude is the maximum amplitude of the signal waveform that characterizes the magnitude of a rock fracture event and is commonly used for fracture source type identification and intensity measurements. And the amplitude distribution is largely dependent on the material and deformation mechanism, so the judgment of the change of rock properties based on the amplitude information is of great significance (Pollock 1973). The amplitude of the signal waveforms is different due to the differences in the AE sources (He et al. 2010; Khoshouei et al. 2022), and the signals with amplitudes in the range of 40–70 dB and 70–100 dB are referred to as low-amplitude and high-amplitude signals (Zhang et al. 2019). The distribution of AE amplitude of basalt after high temperature is shown in Fig. 8, the statistics of AE amplitude is shown in Fig. 8, and the statistics of amplitude mean and proportion of low amplitude are shown in Fig. 9.

From the statistical results of Figs. 8 and 9, it can be seen that the amplitude of the AE signals generated in the fracture process of basalt after high temperature is between 40 and 100 dB, while the proportion of AE events decreases rapidly with the increase of the amplitude. This indicates that small cracks are dominated by low energy damage during rock loading; most of the signals have amplitudes between 40–50 dB, which suggests that the generation of fracture with high energy is resulted from the gradual accumulation of a large number of small fractures. As can be seen in Fig. 9, the AE amplitude distribution characteristics of basalt after heat treatment at different temperatures are similar. Before the plastic strengthening stage, only low amplitude signals are generated, with occasional sudden changes in high amplitude signals. The concentration of high amplitude signals occurs only before and after the peak stress, indicating that high-energy cracks are generated and rock is broken. However, high amplitude energy is already present at the beginning of rock loading when the heat treatment temperature is 1000 °C, which is mainly caused by thermal damage to the rock.

From the results in Fig. 10, it can be seen that the amplitude mean (Fig. 10) and maximum amplitude (Figs. 8, 9) of the AE signals after different temperature effect are different. With the increase of temperature, the amplitude mean of the AE signals are 52 dB, 50 dB, 48 dB, 47 dB, 48 dB and 50 dB, respectively, which also show the "U" shaped change with a decrease followed by an increase, indicating that the energy released during the fracture process of the rock samples after high temperature is decreasing. Meanwhile, the proportions of low amplitude of AE signals are 96.02%, 96.69%, 96.84%, 97.93%, 99.3% and 98.11%, respectively, which are all in larger proportions and with a tendency to increase, which suggests that the effect of temperature on the internal elasticity of the rock samples is greatly reduced, and that the higher the temperature, the more difficult it is to produce large scale fracture. In summary, the AE signals clearly show low amplitude aggregation phenomenon during the fracture process of rock samples under high temperature, that is, with the increase of temperature, the rock samples tend to produce small scale fracture, which is manifested as plastic failure.

3.3 Damage Evolution Analysis of Basalt Fracture Process

3.3.1 Evolution Law of Basalt Fracture Damage under High Temperature

To quantitatively describe the damage evolution law of basalt under temperature and stress, Cho et al. (2015) and Xiao et al. (2009) defined the mechanical

Table 2 Peak and cumulative absolute energy of AE under uniaxial compression of basalt after different thermal temperature

Thermal temperature (°C)	Absolute energy peak (aJ)	Accumulated absolute energy (aJ)
25	3.39E+09	1.48E+10
200	1.20E+09	2.38E+10
400	1.77E+09	6.88E+10
600	3.04E+09	3.72E+10
800	1.22E+09	2.37E+10
1000	5.12E+08	9.72E+09

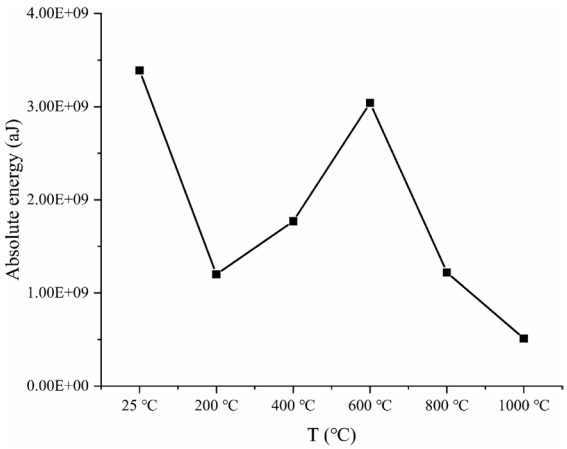

Fig. 6 AE absolute energy peak

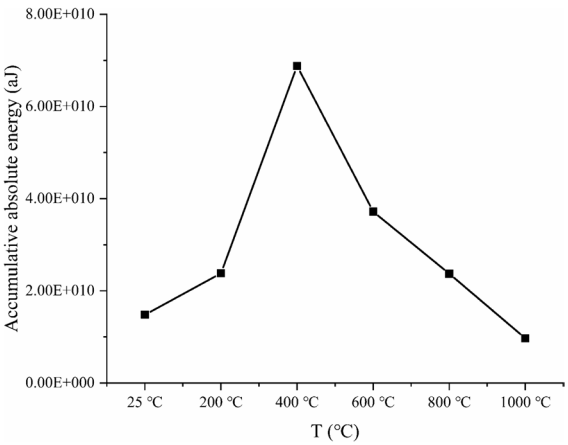

Fig. 7 AE cumulative absolute energy

damage variable of rock samples in compression process based on the AE energy.

$$D_w = \frac{w_t}{w_{AE}} \tag{1}$$

where D_w is the damage variable of basalt at time t. w_t is the AE release energy of rock from the beginning of the test to time t. w_{AE} is the total AE release energy of rock during the whole process from the beginning of the test to reaching the damage limit stress.

In addition, the sample has been subjected to high temperature treatment before the compression test, so there has been some initial damage inside the sample. The initial thermal damage caused by thermal temperature (Ma and Chen 2020) is defined as:

$$D_0 = 1 - \frac{\sigma_T}{\sigma_0} \tag{2}$$

where σ_T is the uniaxial compressive strength of basalt after thermal temperature with the target temperature of T. σ_0 is the uniaxial compressive strength of untreated basalt.

Xu and Karakus (2018) showed that the total damage of rocks after thermal temperature during loading is coupled by initial thermal damage D_0 and mechanical damage D_w according to the following relationship:

$$1 - D = \left(1 - D_0\right)\left(1 - D_w\right) \tag{3}$$

By substituting Eqs. (1) and (2) into Eq. (3), the modified thermal damage variables can be obtained:

$$D = D_0 + D_w - D_0 D_w = 1 - \frac{\sigma_T}{\sigma_0} + \frac{w_t \sigma_T}{w_{AE}\sigma_0} \tag{4}$$

According to Eq. (4), the evolution processes of damage variables in the uniaxial compression of basalt under various conditions are obtained. The damage evolution of basalt under uniaxial compression after high temperature is shown in Fig. 11.

After thermal temperature, the damage variables have similar characteristics. As can be seen from Fig. 11, the high temperature causes certain initial thermal damage to the rock, and the internal cracks of the sample have been developed to a certain extent. According to Eq. (2), the initial damage is 0.012, 0.033, 0.051, 0.152, 0.345 and 0.663, respectively, showing an increasing trend. With the increase of temperature, the damage variable curve gradually

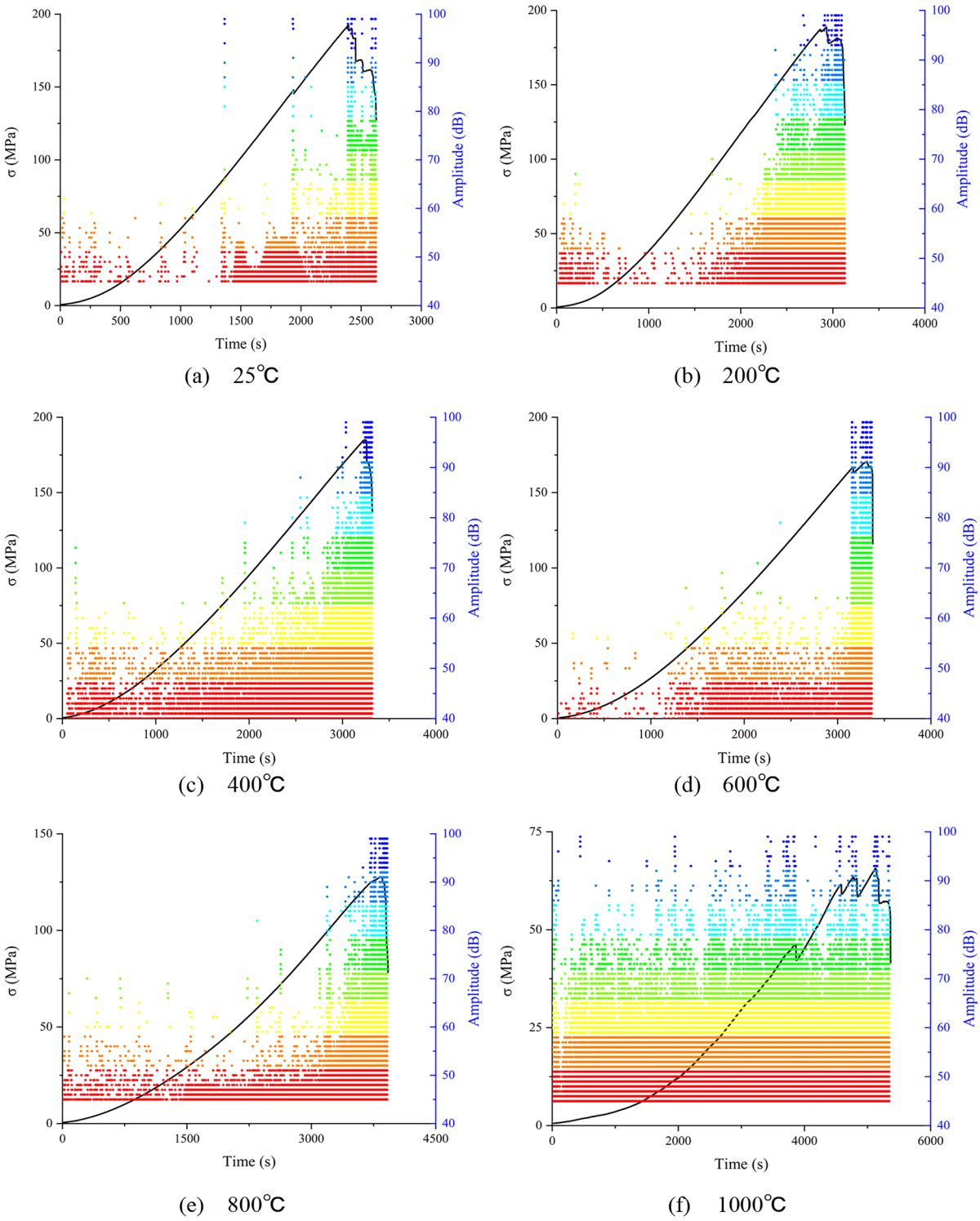

Fig. 8 The distribution of AE amplitude of basalt after high temperature

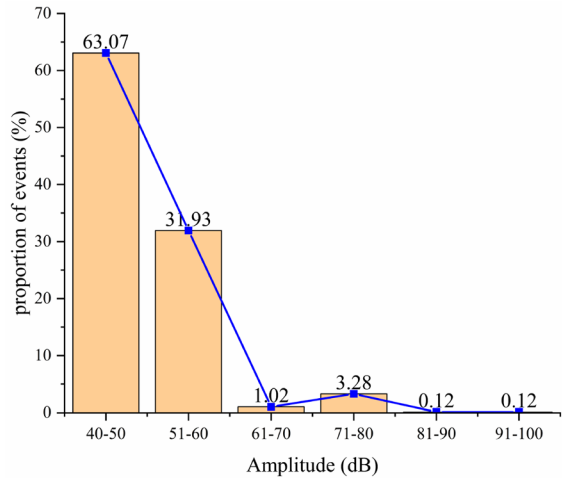

(a) 25°C

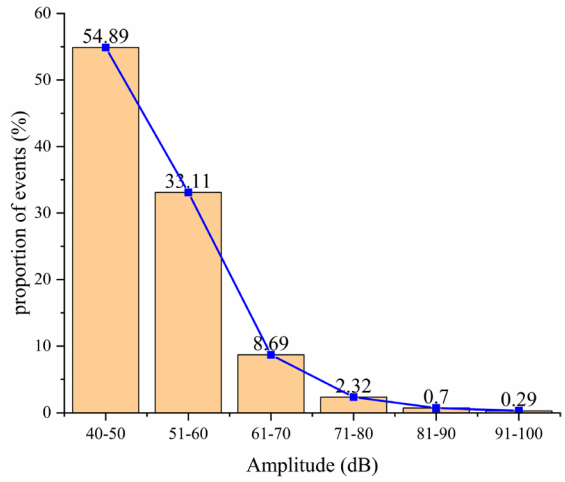

(b) 200°C

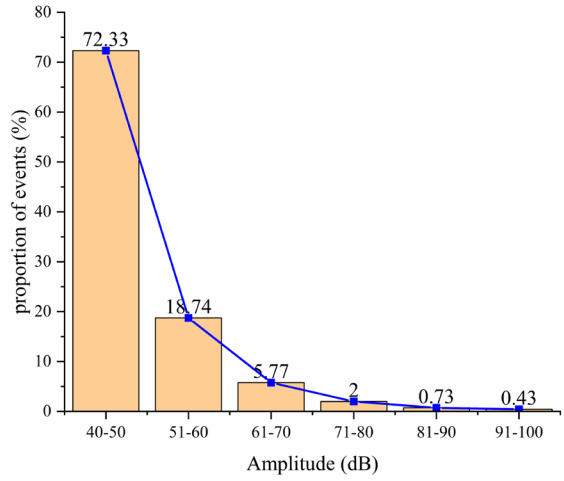

(c) 400°C

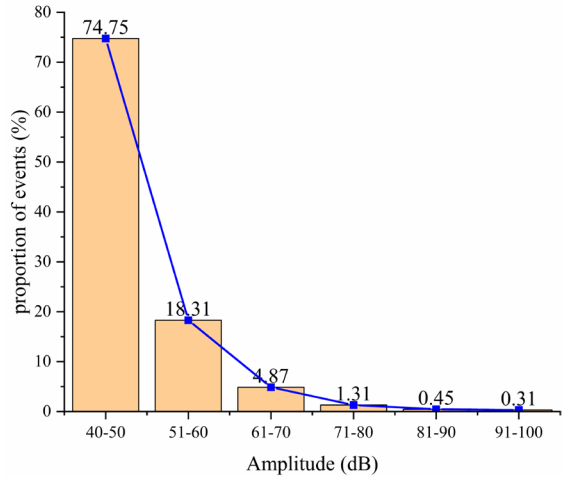

(d) 600°C

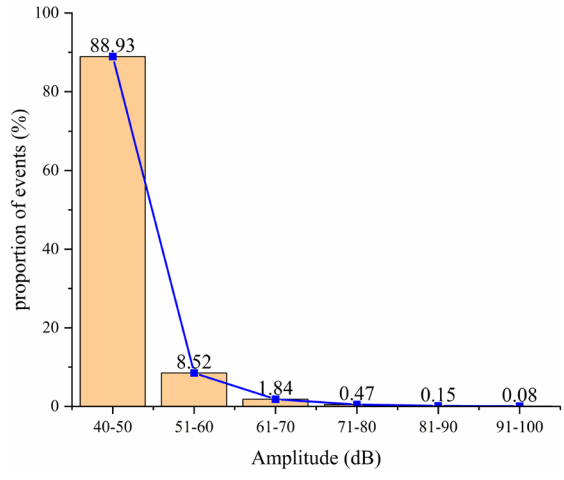

(e) 800°C

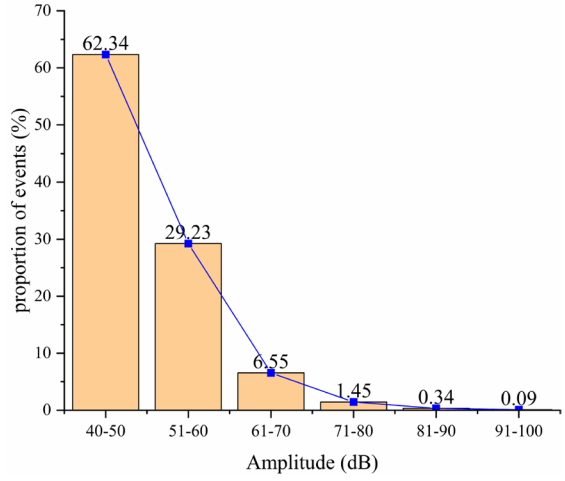

(f) 1000°C

◂**Fig. 9** The statistical of AE amplitude of basalt after high temperature

changes from vertical rise to curve rise, the growth rate slows down, the accelerated damage development stage becomes longer, and the failure characteristics of rock change from brittle failure to plastic failure. Before 800 °C, the initial damage of the rock is relatively small and develops steadily with a certain initial damage. Until the rapid damage development stage, the damage variable rises rapidly until it is equal to the critical value. The rock sample does not appear obvious softening section before the peak stress, but quickly enters the failure section. After the failure, the stress-time curve also declines almost linearly, and the damage variable curve rises linearly, as shown in Fig. 11a–e. However, after 800 °C, the initial damage of rock is large, and the damage variable curve steadily increases with a certain slope. The rock sample has a slight softening characteristic before the peak stress, and the stress-time curve fluctuates after the failure. At the same time, the ductile failure of the rock is the most obvious, as shown in Fig. 11f. After the thermal temperature of 1000 °C, the internal structure of basalt produces thermal damage and forms more dense cracks. A large part of the strain energy accumulated in the process of deformation and failure of the sample in the early stage has been consumed by the crack development and the friction and sliding of crystal particles during the damage failure of the rock. It makes the rock mineral particles slip or even rotate under lower compression load, which is macroscopically manifested as ductile failure of the sample, that is, more obvious strain hardening. The damage variable directly reflects the degree of rock damage through the proportion of microcracks, and well reveals the evolution law of basalt fracture damage under high temperature.

3.3.2 Damage Constitutive Relationship

The theoretical curve can be obtained by bringing the damage variable D obtained by Eq. (4) into the damage constitutive equation. However, considering the effects of physical and mechanical properties such as material anisotropy and the coefficient of thermal expansion, so the damage correction factor (Wang et al. 2021) is introduced, and the damage constitutive equation is as follows.

$$\sigma = E(1 - \eta D)\varepsilon \tag{5}$$

where E is elastic modulus. η is the damage correction factor, which is related to temperature.

The theoretical curve is obtained according to Eq. (5) and it is compared with the test curve, as shown in Fig. 12.

As can be seen from Fig. 12, in the crack closure stage, the stress–strain curve of the model is basically a straight line, which is quite different from the characteristic that the slope gradually becomes larger in the test curve. Because in the crack closure stage, the number of acoustic emission signals generated by the rock is very small relative to the number of acoustic emission signals generated by the entire progressive failure process of the rock, resulting in the ratio w_t/w_{AE} is very small and basically unchanged, so 1–D is approximately constant. As a result, the stress increases linearly with strain at this stage, which is quite different from the experimental results, but the model can reflect the axial stress-axial strain relationship of rock to a certain extent.

Therefore, the selection of the damage correction factor η in the damage constitutive equation of samples under different conditions is reasonable. Different thermal temperature increase the degradation of the damage correction factor η and rock properties, resulting in a decrease in the damage resistance. In addition, before the final failure, when the samples in the same state produce the same strain, the theoretical stress value is greater than the experimental stress value. The main reason for this inconsistency is that the AE sensor cannot receive some AE events with lower energy, indicating that the cracks are small. The theoretical failure value is less than the experimental failure value, so the theoretical stress value obtained from the damage constitutive equation is greater than the experimental stress value.

4 Discussion

4.1 Exploration of Damage Correction Factors

From the above results, it can be seen that the damage evolution of basalt is significantly affected by high temperature. High temperature causes changes in the physical properties of rocks and disruption of the mineral crystal lattice bone of rocks,

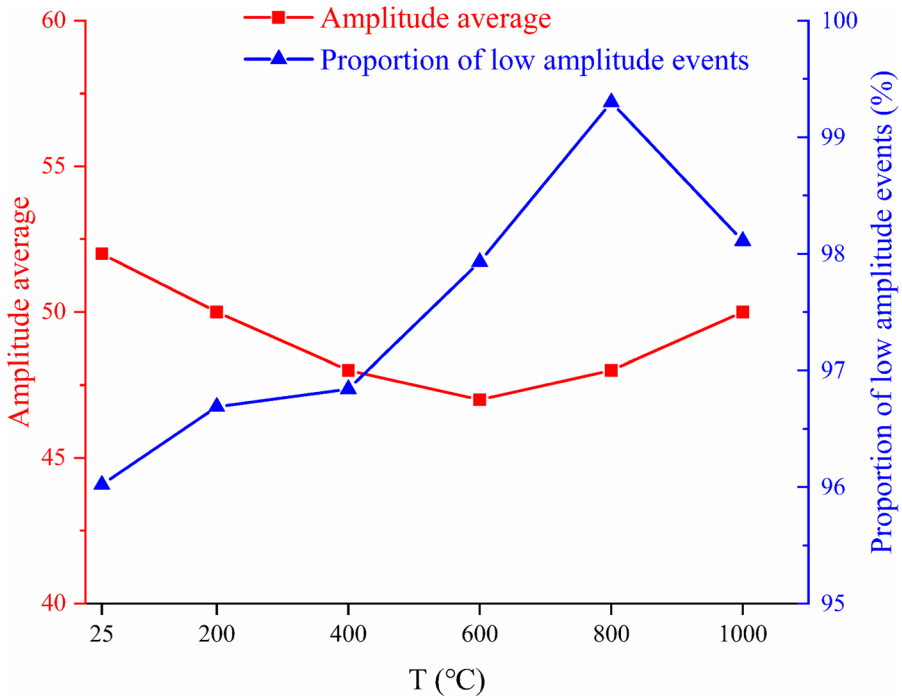

Fig. 10 The statistics of amplitude mean and proportion of low amplitude of basalt after high temperature

leading to cracks and connectivity changes within the rock (Zhang et al. 2018; Heuze 1983; Sun et al. 2016). With the increase of temperature, minerals will expand, melt, phase transform, transform and recrystallize (Sun et al. 2013). In view of the initial damage, the constitutive model based on the damage variable of AE energy can better reflect the mechanical properties of the rock. The selection of damage correction factor in this model has a certain relationship with temperature. By establishing the correlation between the damage correction factor and temperature, it is more convenient to estimate the change of the damage correction factor by the temperature, so as to modify the constitutive model.

The quantitative correlation between the damage correction factor η and temperature in the constitutive model was obtained by fitting, and the correlation coefficient R^2 is 0.99, which represents a good fitting effect. The fitting relation is:

$$\eta = 1.04 - 0.0018 * T + 3.24\exp(-6) * T^2 - 2.10\exp(-9) * T^3, R^2 = 0.99 \quad (6)$$

where η is the damage correction factor; T is the thermal temperature of the basalt.

The correlation between the damage correction factor η and temperature in the present constitutive model is shown in Fig. 13. With the increase of temperature, the damage correction factor η tends to decrease, but there is a change in the rate of change of the curve in the process of change. 200–400 °C, The various forms of water within the rock are evaporated and the mineral lattice begins to change (Heuze 1983; Sun et al. 2013, 2016), resulting in the damage correction factor η beginning to slow with the change of temperature; 600–800 °C, the minerals expand, melt, phase transform, transform and recrystallize, The rock begins to emerge into a liquid state and progressively enters a sintered state (Sun et al. 2013; Chen et al. 2022), resulting in the damage modification factor η beginning to steepen with change of temperature. The future studies could further optimize the damage correction factor η and consider corrections for the nonlinear compaction stage.

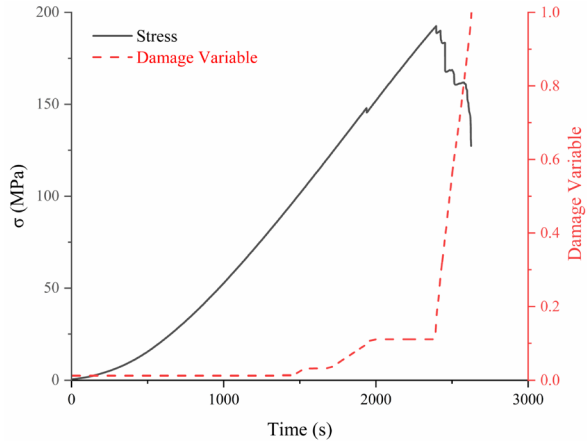

(a) 25 ℃

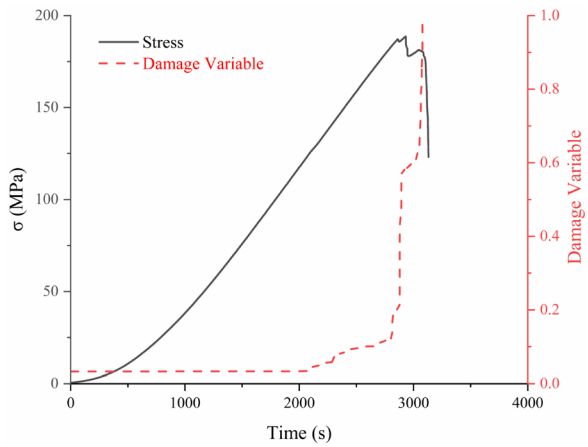

(b) 200 ℃

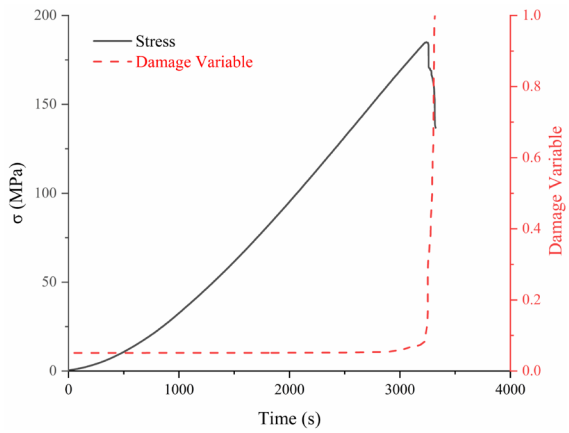

(c) 400 ℃

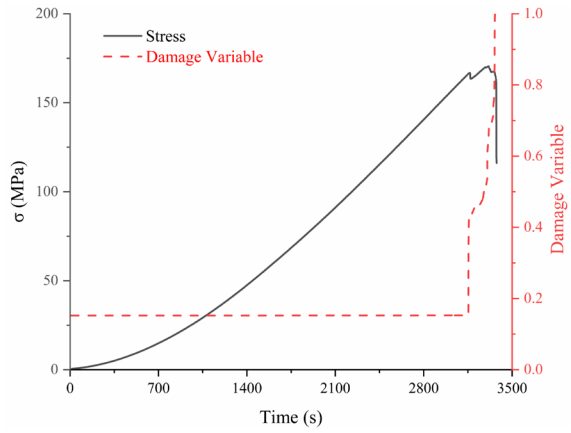

(d) 600 ℃

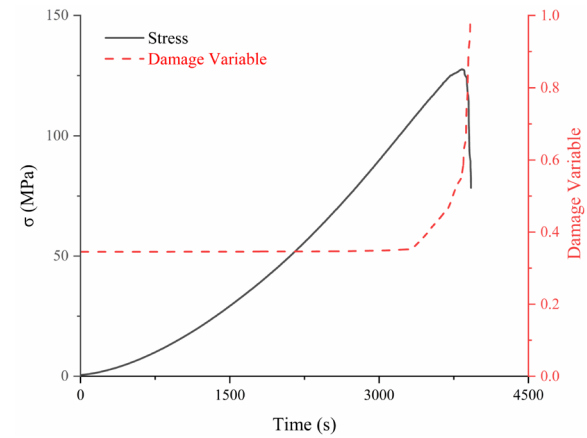

(e) 800 ℃

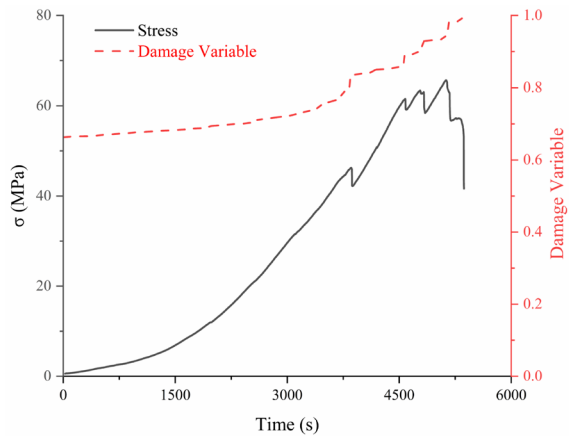

(f) 1000 ℃

Fig. 11 Damage evolution of basalt under uniaxial compression after high temperature

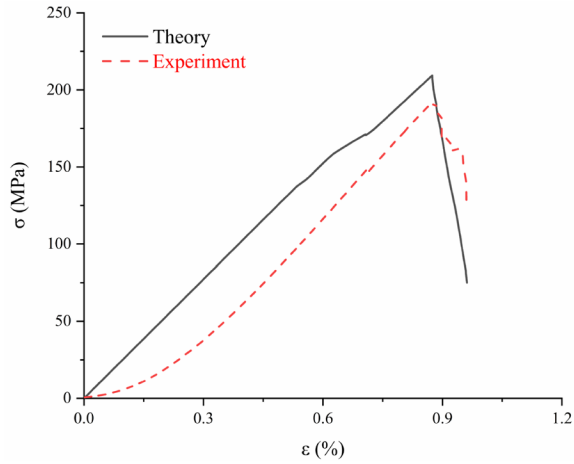

(a) 25 ℃

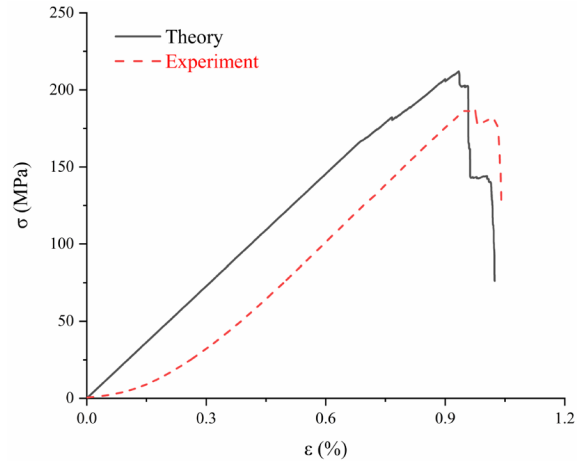

(b) 200 ℃

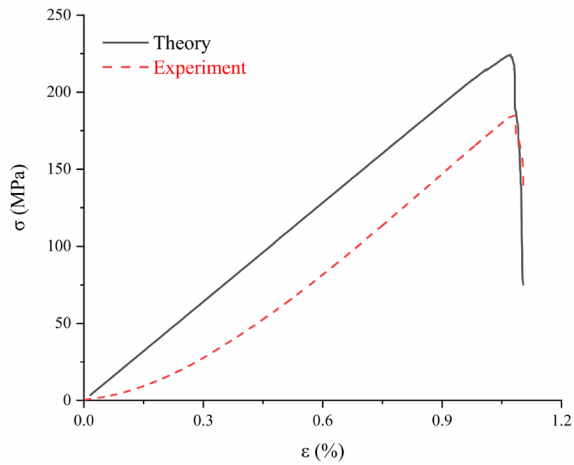

(c) 400 ℃

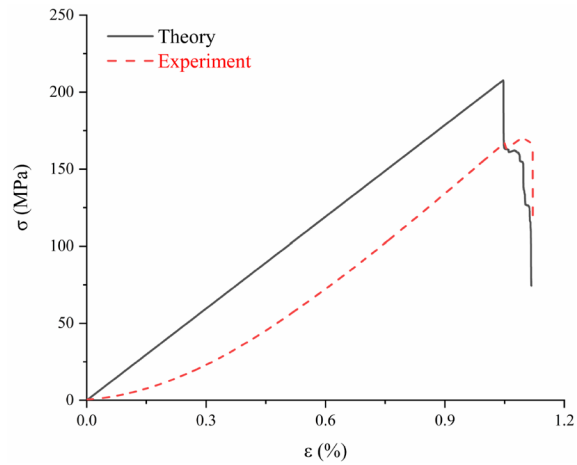

(d) 600 ℃

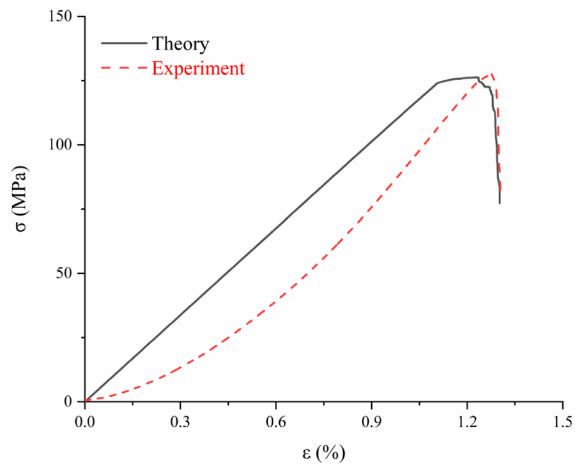

(e) 800℃

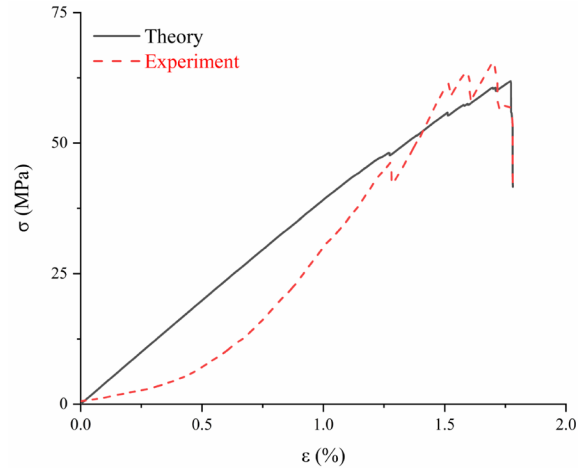

(f) 1000 ℃

◂**Fig. 12** Comparison of theoretical and experimental curves of stress–strain relations of basalt after high temperature

4.2 The Quantitative Error Analysis

The quantitative analysis of error between experimental and theoretical results were shown in Fig. 14. The number marked on the bar chart is the error value of the experimental and theoretical results.

Through the quantitative analysis of the maximum strain and stress error of the experimental and theoretical results, it is found that the maximum strain of the sample is similar, while the maximum stress is only different but also within the controllable range. The errors are 8.05%, 11.92%, 17.51%, 17.86%, 1.07% and 5.74% of the maximum stress, respectively, and the higher the heat treatment temperature, the smaller the error. In addition, we can also find that with the increase of heat treatment temperature, the theoretical stress increases first due to the closure of the original crack and then decreases due to the irreversible rock damage caused by thermal damage, which is similar to the experimental results. Therefore, this model can better describe the mechanical properties of basalt after high temperature uniaxial action, and the higher the heat treatment temperature, the stronger the adaptability of the model.

4.3 Microstructure Characteristics

Basalt is a brittle material formed by dense cementation of various mineral particles. The mineral composition and microstructure together determine the fracture properties of basalt. The difference in mineral composition and microstructure is the internal mechanism that causes the difference in macroscopic mechanical properties. The microstructure, defect morphology and pore structure characteristics of basalt were obtained by scanning electron microscopy, and the fracture mechanism of basalt thermal damage was revealed from the microscopic point of view. The surface microstructure of basalt at different temperatures was observed by scanning electron microscope (SEM), and the results were shown in Fig. 15.

The concave and convex surfaces and folds appear on the surface of the rock, which is mainly caused by the extrusion wear of the particles during the fracture process of the rock, the brittleness of the rock, the heterogeneity of the composition and the uneven distribution of the mineral particles. From the diagram, it can be found that before 400 °C, the fracture of the sample produces typical transgranular fracture characteristics such as parallel cleavage plane and intersecting cleavage plane caused by shear action and smooth cutting surface with parallel slip line stripes or rhyolitic or step-like distribution. After 600 °C, the fracture of the sample produces typical intergranular fracture characteristics such as rough tensile surface and a large number of large rock debris. With the increase of heat treatment temperature, the gloss of the fracture surface decreases and the crack width increases. The fracture of rock tends to be disordered and disordered gradually, and the fracture is not limited to cleavage plane and crystal boundary. Due to the different thermal expansion deformation and stress, there are small pores between crystals and cuttings and other cements. However, with the increase of heat treatment temperature, this boundary becomes blurred, mainly because the minerals in the rock and the cements between the minerals are seriously dried at high temperature.

5 Conclusion

Through uniaxial compression test and AE test of basalt after high temperatures, the relationship between stress–strain curve, AE characteristic parameters and damage evolution characteristics with temperature is analyzed. AE properties and damage characteristics of basalt under high temperature uniaxial stress are revealed. The main conclusions are as follows:

1. The characteristics of stress–strain curve of rock are significantly influenced by temperature. With the increase of temperature, the compaction stage of the curve becomes longer, the plasticity increases, and the peak strength of basalt decreases. The higher the heat treatment temperature, the faster the strength decreases. At 1000 °C, the strength decreases by 63.91% and the local stress fluctuation of the rock sample is obvious and multiple stress drops occur, showing obvious plastic characteristics.
2. The AE spatio-temporal evolution results intuitively reflect the location of the AE source, frac-

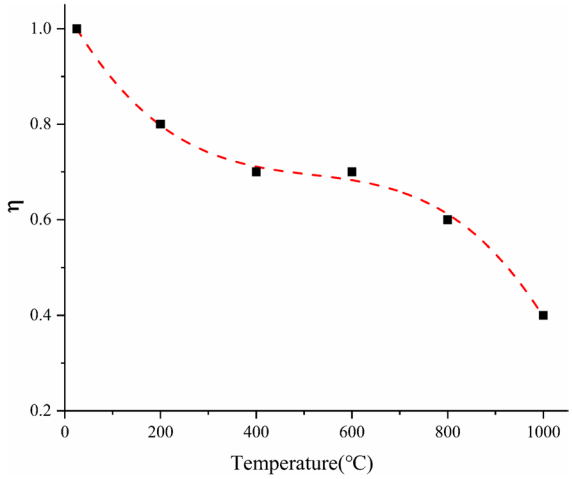

Fig. 13 The correlation between the damage correction factor η and temperature

ture development and damage conditions within the rock. The AE localization points gradually converge from the dispersed state to the aggregated state; With the increase of temperature, the period of convergent nucleation of the AE localization sites is advanced, and the AE absolute energy before the peak stress is fluctuated, and the heat treatment of the rock has an additive effect on the burstiness. High temperature changes the failure pattern of basalt. The failure mechanism of basalt changed from shear failure to tensile-shear mixed failure, and finally to tensile failure. The critical temperature of brittle-ductile transition of basalt is 600–800 °C.

3. The AE characteristic parameters quantify the rock damage and well reflect the damage evolution characteristics of rock samples. The high temperature changes the failure pattern of basalt and has a significant impact on the characteristics of AE signals. With the increase of temperature, the AE absolute energy shows a trend of first decreasing, then increasing and then decreasing, and the turning point of the cumulative absolute AE energy curve is delayed, and there is a "step-like" change; 400–600 °C is the turning point of the decrease of the AE cumulative absolute energy release, and the order of magnitude of energy release decreases at 1000 °C. The high amplitude AE signals shifted from a concentrated distribution near the peak stress to a discrete distribution throughout the entire process, and exhibits a low-amplitude aggregation phenomenon. Based on the variation of acoustic emission characteristic parameters with temperature, the sudden increase of acoustic emission energy, the vertical rise of cumulative acoustic emission absolute energy and the high amplitude acoustic emission signal can be used as the precursory information of rock fracture.

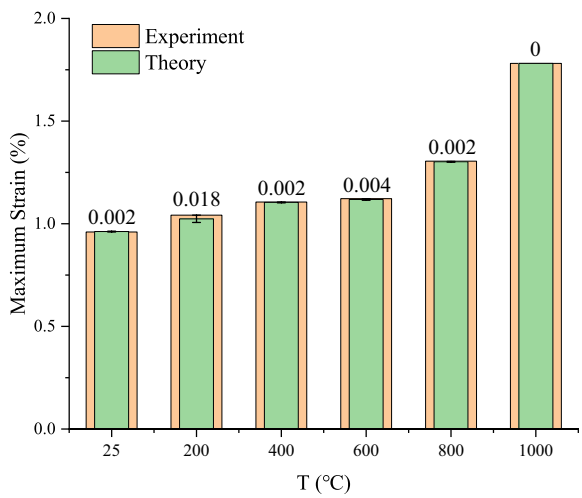

(a) Maximum strain error

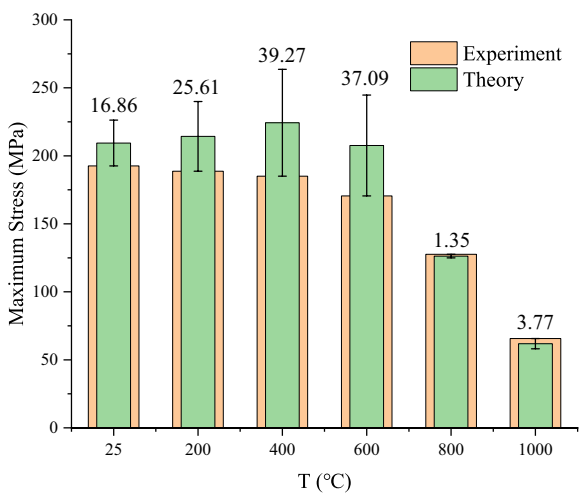

(b) Maximum stress error

Fig. 14 The quantitative analysis of error between experimental and theoretical results

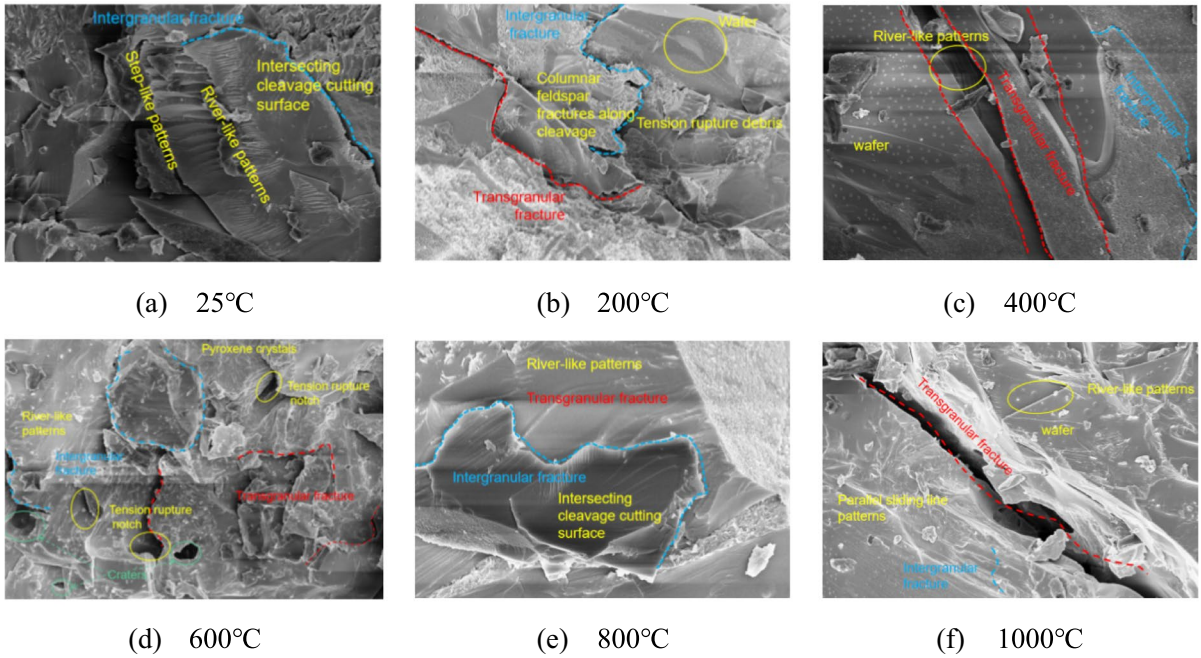

(a) 25℃ (b) 200℃ (c) 400℃

(d) 600℃ (e) 800℃ (f) 1000℃

Fig. 15 SEM scan of basalt samples after high temperature

4. The thermal damage constitutive model considering the coupling of initial thermal damage and mechanical damage is used to simulate the damage characteristics of basalt after high temperature by using the damage correction factor. The validity and applicability of the constitutive model are verified by comparing the experimental results. The influence of high temperature on the damage evolution is discussed. With the increase of temperature, the thermal damage plays a leading role. The evolution of damage variables gradually changes from linear to nonlinear. Before 800 °C, the initial damage is small, the rock damage increases slowly and linearly before the failure, and the near failure increases linearly. The initial damage multiplied after 800 °C, and the damage maintained a certain slope growth, especially at 1000 °C.

Acknowledgements The authors sincerely thank the financial support from the Project supported by Hunan Provincial Natural Science Foundation of China (No.2023JJ30511), Research Foundation of the Department of Natural Resources of Hunan Provincial of China (No.20230144DZ), Educational Commission of Hunan Province of China (Key Program) (No.18A252), Hunan Postgraduate Research Innovation Project (No.QL20220216).

Author Contributions Wenzhao Chen: Formal analysis, Conceptualization, Visualization, Supervision, Funding acquisition. Rong Hu: Investigation, Methodology, Writing-original draft, Funding acquisition. Xiqi Liu: Supervision, Funding acquisition, Writing—review and editing. Gang Wang: Supervision, Writing—review and editing. Bingwen Gong: Writing—review and editing. Yan Chang: Writing—review and editing. Heng Deng: Writing—review and editing. Chunming Qi: Writing—review and editing, Funding acquisition.

Data Availability The datasets generated during and/or analysed during the current study are not publicly available due to reason why data are not public but are available from the corresponding author on reasonable request.

Declarations

Conflict of interest The authors declare that they have no conflict of interest.

Ethical Approval The authors wish to confirm that there are no known conflicts of interest associated with this manuscript.

References

Ali AY, Bradshaw SM (2010) Bonded-particle modelling of microwave-induced damage in ore particles. Miner Eng 23(10):780–790. https://doi.org/10.1016/j.mineng.2010.05.019

Cao RH, Fang L, Qiu XY et al (2022) Damage deterioration mechanism and damage constitutive modelling of red sandstone under cyclic thermal-cooling treatments. Arch Civ Mech Eng. https://doi.org/10.1007/S43452-022-00505-6

Chajed S, Singh A (2024) Microcrack classification of rock salt under quasi-static compression using acoustic emission. Geotech Geol Eng. https://doi.org/10.1007/s10706-024-02752-1

Chen S, Shi XC, Bao H et al (2022) Experimental study on high temperature on the drillability and microstructure of basalt. Chin J Undergr Space Eng 18(06):1898–1905. https://doi.org/10.1673-0836(2022)06-1898-08

Cho GC, Kim JS, Won JC et al (2015) A comparative evaluation of stress strain and acoustic emission methods for quantitative damage assessments of brittle rock. Rock Mech Rock Eng 48(2):495–508. https://doi.org/10.1007/s00603-014-0590-0

Deng LC, Wu Y, Ji YK et al (2022) Physical and mechanical properties of granite after high-temperature and acidic treatment for the enhanced geothermal system. Bull Eng Geol Environ. https://doi.org/10.1007/S10064-022-02928-0

Dong Z, Chen YP, Wang XG et al (2022) Evaluation of thermophysical and mechanical properties of sandstone due to high-temperature. Materials 15(23):8692–8692. https://doi.org/10.3390/ma15238692

Fairhurst CE, Hudson JA (1999) Draft ISRM suggested method for the complete stress-strain curve for intact rock in uniaxial compression. Int J Rock Mech Min Sci Geomech 36(3):281–289. https://doi.org/10.1016/S0148-9062(99)00006-6

GB/T 50266-2013, Standard for test methods of engineering rock mass. Beijing China Planning Publishing House, Beijing

Hakan E, Hasan K, Murat K et al (2019) Effect of thermal damage on mineralogical and strength properties of basic volcanic rocks exposed to high temperatures. Bull Eng Geol Environ. https://doi.org/10.1007/s10064-017-1208-z

He MC, Miao JL, Feng JL (2010) Rock burst process of limestone and its acoustic emission characteristics under true-triaxial unloading conditions. Int J Rock Mech Min Sci 47(2):286–298. https://doi.org/10.1016/j.ijrmms.2009.09.003

Heuze FE (1983) High-temperature mechanical, physical and thermal propertiesof granitic rocks-a review. Int J Rock Mech Min Sci 20(1):3–10. https://doi.org/10.1016/0148-9062(83)91609-1

Horst W (2019) Deep mining: a rock engineering challenge. Rock Mech Rock Eng. https://doi.org/10.1007/s00603-019-01799-4

Hrifech S, Bennouna EG, Faik A et al (2023) Experimental assessment of quartz-rich rocks as storage materials for medium and high temperatures air packed bed system. J Energy Storage 70:107849. https://doi.org/10.1016/j.est.2023.107849

Jobmann M, Wilsnack T, Voigt HD (2010) Investigation of damage-induced permeability of Opalinus clay. Int J Rock Mech Min Sci 47(2):279–285. https://doi.org/10.1016/j.ijrmms.2009.11.009

Ju W (2010) High-level radioactive waste disposal in China: update 2010. J Rock Mech Geotech Eng. https://doi.org/10.3724/SP.J.1235.2010.00001

Justo J, Castro J (2020) Mechanical properties of 4 rocks at different temperatures and fracture assessment using the strain energy density criterion. Geomech Energy Environ. https://doi.org/10.1016/j.gete.2020.100212

Khadivi B, Heidarpour A, Zhang QB et al (2023) Characterizing the cracking process of various rock types under Brazilian loading based on coupled Acoustic Emission and high-speed imaging techniques. Int J Rock Mech Min Sci 168:105417. https://doi.org/10.1016/j.ijrmms.2023.105417

Khoshouei M, Bagherpour R, Jalalian MH (2022) Rock type identification using analysis of the acoustic signal frequency contents propagated while drilling operation. Geotech Geol Eng 40(3):1237–1250. https://doi.org/10.1007/s10706-021-01957-y

Kitamura A, Doi R, Yoshida Y (2011) Evaluated and estimated solubility of some elements for performance assessment of geological disposal of high-level radioactive waste using updated version of thermodynamic database. In: Proceedings of the 13th international conference on environmental remediation and radioactive waste management, vol 2, pp 365–373. https://doi.org/10.1115/ICEM2010-40172

Kumari WGP, Ranjith PG, Perera MSA, et al (2017) Mechanical behaviour of Australian Strathbogie granite under in-situ stress and temperature conditions: an application to geothermal energy extraction. Geothermics. https://doi.org/10.1016/j.geothermics.2016.07.002

Kwon S, Choi JW (2006) Thermo-mechanical stability analysis for a multi-level radioactive waste disposal concept. Geotech Geol Eng 24:361–377. https://doi.org/10.1007/s10706-004-7935-5

Li HR, Wang ZH, Meng SR et al (2021) Acoustic emission activity and damage evolution characteristics of marble under triaxial stress at high temperatures. Rock Soil Mech 42(10):2672–2682. https://doi.org/10.16285/j.rsm.2021.0253

Li X, Wang XQ, Wang KY et al (2022) Damage evolution of rocks containing a set of cross-Joints based on acoustic emission characteristics. Adv Mater Sci Eng. https://doi.org/10.1155/2022/4120287

Luc LNM, Joseph N, Jean MBN (2015) Modeling and numerical analysis of granite rock specimen under mechanical loading and fire. J Rock Mech Geotech Eng. https://doi.org/10.1016/j.jrmge.2014.07.007

Ma B, Chen HY (2020) Acoustic emission characteristics and damage evolution of granite after elevated temperature. Min Res Dev 40(1):22–27. https://doi.org/10.13827/j.cnki.kyyk.2020.01.005

Manish KJ, Verma AK, Pradeep KG et al (2017) Study of mechanical properties of Vindhayan shaly rocks at

elevated temperature. J Geol Soc India. https://doi.org/10.1007/s12594-017-0714-8
Motra HB, Stutz HH (2018) Geomechanical rock properties using pressure and temperature dependence of elastic P- and S-wave velocities. Geotech Geol Eng 36(6):3751–3766. https://doi.org/10.1007/s10706-018-0569-9
Nakayama S, Watanabe Y, Kato M (2011). Regulatory research for geological disposal of high-level radioactive waste in Japan. In: Proceedings of the 13th international conference on environmental remediation and radioactive waste management, vol 2, pp 279–285. https://doi.org/10.1115/ICEM2010-40116
Ozguven A, Ozcelik Y (2013) Investigation of some property changes of natural building stones exposed to fire and high heat. Constr Build Mater. https://doi.org/10.1016/j.conbuildmat.2012.09.072
Pollock AA (1973) Acoustic emission-2: acoustic emission amplitudes. Non-Destr Test 6(5):264–269. https://doi.org/10.1016/0029-1021(73)90074-1
Ren MY, Zhang QY, Liu CC et al (2019) The elastic-plastic damage analysis of underground research laboratory excavation for disposal of high level radioactive waste. Geotech Geol Eng 37:1793–1811. https://doi.org/10.1007/s10706-018-0723-4
Rong G, Peng J, Cai M et al (2018) Experimental investigation of thermal cycling effect on physical and mechanical properties of bedrocks in geothermal fields. Appl Therm Eng 141:174–185. https://doi.org/10.1016/j.applthermaleng.2018.05.126
Sagar VR, Prasad RKB (2012) A review of recent developments in parametric based acoustic emission techniques applied to concrete structures. Nondestruct Test Eval 27(1):47–68. https://doi.org/10.1080/10589759.2011.589029
Singalreddy SP, Cui L, Fang K (2022) Spatiotemporal evolution of thermo-hydro-mechanical-chemical processes in cemented paste backfill under interfacial loading. Int J Min Sci Technol. https://doi.org/10.1016/j.ijmst.2022.10.002
Sun Q, Zhang ZZ, Xue L et al (2013) Physico-mechanical properties variation of rock with phase transformation under high temperature. Chin J Rock Mech Eng 32(5):935–942. https://doi.org/10.3969/j.issn.1000-6915.2013.05.011
Sun Q, Lu C, Cao L et al (2016) Thermal properties of sandstone after treatment at high temperature. Int J Rock Mech Min Sci 85:60–66. https://doi.org/10.1016/j.ijrmms.2016.03.006
Thomas HP (1983) The national research council, study of the isolation system for geologic disposal of radioactive wastes. MRS Proc. https://doi.org/10.1557/PROC-26-461
Ullah B, Zhou ZL, Cai X et al (2023) Failure prediction and microcracks development based on acoustic emission and energy evolution for different rocks treated with freeze–thaw weathering. Bull Eng Geol Environ. https://doi.org/10.1007/s10064-023-03485-w
Vagnon F, Colombero C, Comina C et al (2021) Relating physical properties to temperature induced damage in carbonate rocks. Géotech Lett 11(2):147–157. https://doi.org/10.1680/JGELE.20.00122
Víctor M, Elvira GM, Carlos HS et al (2021) Thermal effects on the drilling performance of a limestone: relationships with physical and mechanical properties. Appl Sci 11(7):3286–3286. https://doi.org/10.3390/APP11073286
Wang HJ, Li J, Guo Q et al (2021) Experimental study on the influence of water on the failure properties of sandstone. Bull Eng Geol Environ. https://doi.org/10.1007/S10064-021-02410-3
Wang G, Luo Y, Gong HL et al (2023) Investigations on the macro-meso mechanical properties and energy dissipation mechanism of granite shear fracture under dynamic disturbance. Int J Numer Anal Methods Geomech. https://doi.org/10.1002/nag.3584
Xiao JQ, Ding DX, Jiang FL et al (2009) Fatigue damage variable and evolution of rock subjected to cyclic loading. Int J Rock Mech Min Sci. https://doi.org/10.1016/j.ijrmms.2009.11.003
Xie ZW, Ling SX, Liao X et al (2023) Study on the weightless-expansion mechanism of red-layer mudstone at different heat treatment temperatures. J Rock Mech Geotech Eng 42(01):154–167. https://doi.org/10.13722/j.cnki.jrme.2022.0371
Xu XL, Karakus M (2018) A coupled thermo-mechanical damage model for granite. Int J Rock Mech Min Sci 103:195–204. https://doi.org/10.1016/j.ijrmms.2018.01.030
Xue Y, Liu J, Liang X et al (2021) Nonlinear evolution characteristics of acoustic emission and fracture mechanism of coal under gas pressure. Chin J Geotech Eng 43(S1):241–245
Yin TB, Ma JX, Wu Y et al (2022) Effect of high temperature on the brittleness index of granite: an experimental investigation. Bull Eng Geol Environ. https://doi.org/10.1007/S10064-022-02953-Z
Zhang W, Sun Q, Zhang Y et al (2018) Porosity and wave velocity evolution ofgranite after high-temperature treatment; a review. Environ Earth Sci 77(9):1–13. https://doi.org/10.1007/s12665-018-7514-3
Zhang YB, Zhang H, Liang P et al (2019) Experimental research on time-frequency characteristics of AE P-wave and S-wave of granite under failure process. Chin J Rock Mech Eng. https://doi.org/10.13722/j.cnki.jrme.2019.0250
Zhao J (1994) Geothermal testing and measurements of rock and rock fractures. Geothermics. https://doi.org/10.1016/0375-6505(94)90001-9